

# Non-Fermi-liquid transport phenomena in bilayer nickelates: Impact of quasi-quantum metric

Seiichiro Onari<sup>1</sup>, Daisuke Inoue<sup>1</sup>, Rina Tazai<sup>2</sup>, Youichi Yamakawa<sup>1</sup>, and Hiroshi Kontani<sup>1</sup>

<sup>1</sup>*Department of Physics, Nagoya University, Nagoya 464-8602, Japan*

<sup>2</sup>*Yukawa Institute for Theoretical Physics, Kyoto University, Kyoto 606-8502, Japan*

(Dated: August 27, 2025)

Recently discovered high- $T_c$  superconductivity in thin-film bilayer nickelates  $\text{La}_3\text{Ni}_2\text{O}_7$  under ambient pressure has attracted great interest. Non-Fermi-liquid transport behaviors, such as  $T$ -linear resistivity and positive Hall coefficient increasing at low temperatures, have been reported in this system. In this study, we analyze the non-Fermi-liquid transport phenomena in the thin-film bilayer nickelate  $\text{La}_3\text{Ni}_2\text{O}_7$  using a multiorbital tight-binding model. In  $\text{La}_3\text{Ni}_2\text{O}_7$ , the orbital-selective cold spots composed of Ni  $d_{x^2-y^2}$  orbital emerge since the spin fluctuations cause stronger quasi-particle damping  $\gamma$  in the Ni  $d_{x^2-y^2}$  orbital. Notably, in the present study, we derive a rigorous formula for the Hall coefficient  $R_H$  incorporating the  $\gamma$  in the quasi-quantum metric (qQM) term. We discover that the  $T$ -dependence of  $\gamma$  in the qQM term is important in determining  $R_H$ , and that the qQM term is inevitably enhanced by the nearly degenerate bands at the orbital-selective cold spots located around  $(\pi/4, \pi/4)$ . Moreover, the qQM term plays an essential role in describing the Nernst coefficient and other transport phenomena involving the second derivative velocity  $v^{\mu\nu}$ .  $\text{La}_3\text{Ni}_2\text{O}_7$  provides a novel platform for exploring the physics of the qQM.

## I. INTRODUCTION

The recent discovery of high- $T_c$  superconductivity in thin-film  $\text{La}_3\text{Ni}_2\text{O}_7$  under ambient pressure has generated significant interest. The realized superconducting (SC) transition temperature ( $T_c$ ) is about 40K [1–4]. The phase diagram of this system has not been clear yet. ARPES measurements propose  $\sim 20\%$  hole-doping for each Ni atom, and the epitaxial strain is introduced in the thin-film system [5]. On the other hand, in bulk samples, superconductivity with  $T_c \sim 80\text{K}$  under  $P \sim 10\text{GPa}$  has been reported [6–8]. At ambient pressure of the bulk sample, double-stripe spin density wave (SDW) with  $\mathbf{q}_s \approx (\pi/2, \pm\pi/2)$  appears at  $T_{\text{sdw}} \approx 150\text{K}$  [9–16]. Furthermore, the charge density wave (CDW) orders have been observed at the CDW transition temperature  $T_{\text{cdw}}$  comparable to  $T_{\text{sdw}}$  [10–19].

To understand the mechanism of the SC state, it is important to elucidate the parent normal states. The non-Fermi-liquid transport phenomena are evidence of strongly correlated electron systems. In proximity to the quantum-critical point of the SDW or CDW, non-Fermi-liquid transport phenomena have been observed in infinite-layer nickelates, Fe-based, and cuprate superconductors [20–31]. Very recently, in thin-film bilayer nickelate, the non-Fermi-liquid behaviors of the resistivity  $\rho \propto T$  and the positive Hall coefficient  $R_H$  increasing at low temperatures have been reported [1, 4].

The origin of  $T$ -dependent  $R_H$  has been proposed to be (i) the  $\mathbf{k}$  and band dependences of quasi-particle damping  $\gamma$  [32] and (ii) the current vertex corrections (CVC) [26–31] in cuprates and Fe-based superconductors. In mechanism (i), a significantly large anisotropy of  $\gamma$  is required to account for the  $T$ -dependent  $R_H$  observed in experiments. In contrast, the  $T$ -dependent  $R_H$  is naturally explained by the total current  $J$  affected by the backward scatterings from the CVC in mechanism (ii).

In the present study, we propose a novel third mechanism (iii) “the quasi-quantum metric (qQM) mechanism”, which is significant when the bands are degenerate as in  $\text{La}_3\text{Ni}_2\text{O}_7$ . In this mechanism, the  $T$ -dependence of  $\gamma$ , incorporated into the newly derived qQM term formula in the present study, plays a critical role. The qQM and QM are the paramount concepts in condensed matter physics. We discover that the qQM, including the many-body effects, is important for the  $T$ -dependent  $R_H$ .

Previous theoretical studies on bulk and thin-film  $\text{La}_3\text{Ni}_2\text{O}_7$  have proposed spin-fluctuation-mediated SC states with sign-reversing gaps, such as  $d$ -wave and  $s\pm$ -wave states [33–48] have been proposed. The normal and SC states have also been studied by employing strong coupling approaches [33, 45, 49–53]. Importantly, we have recently revealed that both inter-layer and intra-layer CDW instabilities emerge concurrently with the SDW instability. This CDW can be explained by the paramagnon-interference (PMI) mechanism [54]. However, the non-Fermi-liquid transport phenomena remain unsolved. A novel theory is required to address this issue.

In this study, we study the origin of non-Fermi-liquid transport phenomena in thin-film bilayer nickelate  $\text{La}_3\text{Ni}_2\text{O}_7$  by focusing on many-body effects on the qQM term within a 2D multiorbital tight-binding model. In  $\text{La}_3\text{Ni}_2\text{O}_7$ , the orbital-selective cold spots emerge due to the orbital dependence of  $\gamma$ , which is driven by the spin fluctuations. For simplicity, we ignore the CDW fluctuations and the CVC. We derive a novel formula for the  $R_H$  that incorporates the many-body effects on the qQM. We discover that the qQM term inevitably becomes significant in  $\text{La}_3\text{Ni}_2\text{O}_7$  since the bands are nearly degenerate at the orbital-selective cold spots. The obtained  $\rho \propto T$  and the enhancement of positive  $R_H$  at low  $T$  are consistent with experimental observations [1, 4]. We also obtain the negative Nernst and Seebeck coefficients, which have not yet been experimentally observed in thin-film

La<sub>3</sub>Ni<sub>2</sub>O<sub>7</sub>.

## II. NOVEL FORMULA OF HALL COEFFICIENT

Here we derive a rigorous formula for the normal Hall conductivity  $\sigma_{xy}$  in “multiorbital tight-binding models” based on the Green function method. This is an extension of the study for single-orbital models in Ref. [55] to multiorbital models, where finite QM and qQM exist. The obtained  $\sigma_{xy}$  contains the qQM term, which can exhibit a prominent temperature dependence in strongly correlated metals. Importantly, the effect of the self-energy on the qQM, which should be significant in strongly correlated metals, is derived accurately.

In Ref. [56], three of the present authors (R.T., Y.Y., and H.K.) have revealed a significant role of the QM in the electronic magnetochiral anisotropy (eMChA), a non-reciprocal transport phenomenon of order  $E^2B$  in the electric and magnetic fields. In the loop-current phase in kagome metals, the derived eMChA conductivity takes a huge value proportional to  $\tau^3$ , where  $\tau$  is the lifetime of electrons. Significantly, the eMChA is strongly magnified ( $\sim 100$  times) by the QM term in multiorbital kagome metals, giving rise to the giant eMChA discovered in kagome metals [57]. This study demonstrates the significance of the QM term in multiorbital systems.

In the following, we study the multiorbital tight-binding model:

$$H = \sum_{i\alpha, j\beta, \sigma} t_{i\alpha, j\beta} c_{i\alpha, \sigma}^\dagger c_{j\beta, \sigma}, \quad (1)$$

where  $i, j$  represent the indices of the unit-cell ( $i = 1 \sim N$ ), and  $\alpha, \beta$  represent the site and/or orbital in each unit-cell ( $\alpha = 1 \sim M$ ).  $\sigma$  is the spin index. In the present La<sub>3</sub>Ni<sub>2</sub>O<sub>7</sub> model,  $M = 4$ . In the momentum space, Eq. (1) is rewritten as

$$H = \sum_{\mathbf{k}, \alpha, \beta, \sigma} h_{\mathbf{k}}^{\alpha, \beta} c_{\mathbf{k}\alpha, \sigma}^\dagger c_{\mathbf{k}\beta, \sigma}. \quad (2)$$

Here,  $\hat{h}_{\mathbf{k}}$  is the Hamiltonian matrix in the orbital representation. The eigenvalue equation of  $\hat{h}_{\mathbf{k}}$  is

$$\hat{h}_{\mathbf{k}} |u_{a, \mathbf{k}}\rangle = \epsilon_{a, \mathbf{k}} |u_{a, \mathbf{k}}\rangle, \quad (3)$$

where  $\epsilon_{a, \mathbf{k}}$  is the  $a$ -th band-energy ( $a = 1 \sim M$ ), and  $|u_{a, \mathbf{k}}\rangle$  represents the Bloch function. Hereafter, we will refer to the conduction band as  $a$  and the valence band as  $b$ .

The  $xy$ -plane Hall conductivity under  $\mathbf{B} \parallel \mathbf{e}_z$  is defined as

$$j_x = \sigma_{xy} E_y B_z. \quad (4)$$

According to the standard perturbation theory,

$$\sigma_{xy} = - \frac{\partial^2}{i\partial\omega\partial B_z} K(\omega) \Big|_{\omega=B_z=0}, \quad (5)$$

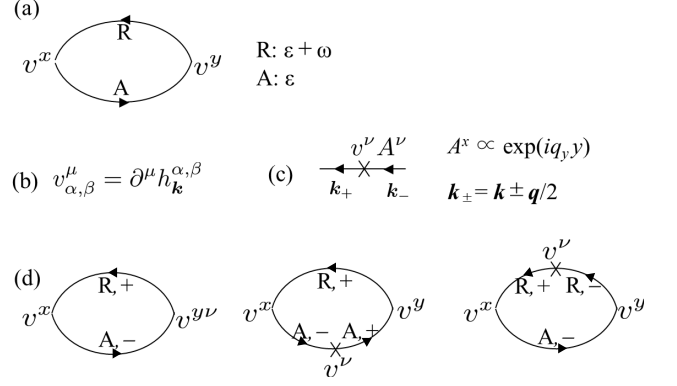


FIG. 1. (a) Current correlation function  $K(i\omega_l)$ . (b) Velocity  $v^\mu$  in the orbital representation  $(\alpha, \beta)$ . (c)  $A_\nu$ -linear term derived from the Green function, where  $\mathbf{q}$  is the momentum of the vector potential and  $\mathbf{k}_\pm \equiv \mathbf{k} \pm \mathbf{q}/2$ . (d)  $A_\nu$ -linear term of (a), composed of two or three Green functions.

where  $\omega$  is the frequency of the electric fields  $E_y$ .  $K(\omega)$  is given by the analytic continuation of the current correlation function  $K(i\omega_l)$ :

$$K(i\omega_l) = g_s T \sum_n \text{Tr} \{ \hat{v}^x \hat{G}^R \hat{v}^y \hat{G}^A \}, \quad (6)$$

which is expressed in Fig. 1 (a). Here,  $\text{Tr}$  represents the summations of orbital indices and momenta.  $\hat{v}$  is the velocity operator and  $\hat{G}$  is the Green function for finite  $\mathbf{A}$ ,  $R$  ( $A$ ) represent the frequency  $\epsilon_n + \omega_l$  ( $\epsilon_n$ ), and  $g_s$  is the spin degeneracy 2.

To extract the  $B_z$ -linear term from Eq. (6), we introduce the vector potential  $\mathbf{A}_{\mathbf{q}} = \mathbf{A}_0 e^{i\mathbf{q} \cdot \mathbf{r}}$ , and take the limit  $|\mathbf{q}| \rightarrow 0$  at the final stage of the calculation [29, 55]. Then, the uniform magnetic field is  $\mathbf{B} = [\text{rot} \mathbf{A}_{\mathbf{q}}]_{\mathbf{q}=0} = [i\mathbf{q} \times \mathbf{A}_{\mathbf{q}}]_{\mathbf{q}=0}$ , or equivalently  $B^\mu = [\epsilon^{\mu\eta\nu} \partial^\eta A^\nu_{\mathbf{q}}]_{\mathbf{q} \rightarrow 0} = [\epsilon^{\mu\eta\nu} (iq_\eta) A^\nu_0]_{\mathbf{q} \rightarrow 0}$ , where  $|\mathbf{A}_0| = |\mathbf{B}|/|\mathbf{q}|$ . For example,  $\mathbf{B} = (0, 0, B_z)$  is obtained when  $\mathbf{q} = (0, q_y, 0)$  and  $\mathbf{A}_0 = (B_z/iq_y, 0, 0)$ . Then, the  $\mathbf{A}$ -linear potential in the orbital basis is

$$H' = e A_0^\nu \sum_{\mathbf{k}} \hat{c}_{\mathbf{k}-}^\dagger \hat{v}_{\mathbf{k}}^\nu \hat{c}_{\mathbf{k}+}, \quad (7)$$

which are shown in Figs. 1 (b) and (c). Here,  $\hat{v}_{\mathbf{k}}^\nu \equiv \partial^\nu \hat{h}_{\mathbf{k}}$ , where  $\partial^\nu$  denotes  $\frac{\partial}{\partial k_\nu}$ ,  $\mathbf{k}_\pm \equiv \mathbf{k} \pm \mathbf{q}/2$ , and  $-e$  ( $e > 0$ ) is the carrier of an electron. We can also show the following relations up to  $O(q^1)$ :

$$\hat{G}_{\mathbf{k}\pm} = \hat{G}_{\mathbf{k}} \pm \frac{1}{2} \hat{G}_{\mathbf{k}} \hat{v}_{\mathbf{k}}^\mu \hat{G}_{\mathbf{k}} \cdot q_\mu, \quad (8)$$

$$\hat{v}_{\mathbf{k}\pm}^\mu = \hat{v}_{\mathbf{k}}^\mu \pm \frac{1}{2} \hat{v}_{\mathbf{k}}^{\mu\nu} \cdot q_\nu, \quad (9)$$

where  $\hat{v}_{\mathbf{k}}^{\mu\nu} \equiv \partial^\nu \hat{v}_{\mathbf{k}}^\mu$ . Thus, the  $A$ -linear term of Eq. (6) is given as

$$K^{(1)}(i\omega_l) = A_0^\nu g_s T \sum_{\mathbf{k}, n} \text{tr} \{ \hat{v}_{\mathbf{k}}^x \hat{G}_{\mathbf{k}+}^R \hat{v}_{\mathbf{k}}^{y\nu} \hat{G}_{\mathbf{k}-}^A \}$$

$$\begin{aligned}
& +\hat{v}_{\mathbf{k}}^x \hat{G}_{\mathbf{k}+}^{\text{R}} \hat{v}_{\mathbf{k}+}^y \hat{G}_{\mathbf{k}+}^{\text{A}} \hat{v}_{\mathbf{k}}^{\nu} \hat{G}_{\mathbf{k}-}^{\text{A}} \\
& +\hat{v}_{\mathbf{k}}^x \hat{G}_{\mathbf{k}+}^{\text{R}} \hat{v}_{\mathbf{k}}^{\nu} \hat{G}_{\mathbf{k}-}^{\text{R}} \hat{v}_{\mathbf{k}-}^y \hat{G}_{\mathbf{k}-}^{\text{A}} \}, \quad (10)
\end{aligned}$$

where  $\text{tr}$  represents the summation of orbital indices. This is diagrammatically expressed in Fig. 1 (d). Here,  $\hat{G}_{\mathbf{k}} \equiv (i\epsilon_n \hat{1} - \hat{h}_{\mathbf{k}})^{-1}$  is the  $M \times M$  electron Green function.

Next, we derive the expression of  $\sigma_{xy}$  from Eq. (10), by extracting the  $q$ -linear term and performing the analytic continuation ( $i\omega_l \rightarrow \omega + i\delta$ ) [29, 55]. Finally, we convert the obtained expression to the band-basis. In the band-basis, the Green function is diagonal:  $G_a^{\text{R}}(\epsilon) = (\epsilon - \epsilon_{a,\mathbf{k}} + i\gamma_a)^{-1}$ . The velocities in the orbital basis are converted to the those in the band basis ( $a, b$ ) as  $v_{ab,\mathbf{k}}^{\mu} \equiv \langle u_{a,\mathbf{k}} | \hat{v}_{\mathbf{k}}^{\mu} | u_{b,\mathbf{k}} \rangle$ , and  $\bar{v}_{ab,\mathbf{k}}^{\mu\nu} \equiv \langle u_{a,\mathbf{k}} | \hat{v}_{\mathbf{k}}^{\mu\nu} | u_{b,\mathbf{k}} \rangle$ . We stress that relation  $v_{aa,\mathbf{k}}^{\mu} = \partial^{\mu} \epsilon_{a,\mathbf{k}}$  holds.

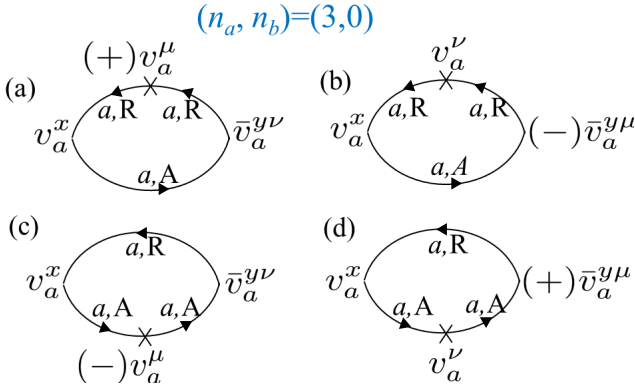


FIG. 2.  $(n_a, n_b) = (3, 0)$  terms for  $\sigma_{xy}$ , derived from the  $A^{\nu} q^{\mu}$ -linear terms from  $K(i\omega_l)$ .  $a$  represents the conduction band.

The derived expression of  $\sigma_{xy}$  are composed of  $(G_a)^{n_a} \times (G_b)^{n_b}$ -terms with  $n_a + n_b = 3$  or 4, where  $a$  is the conduction band and  $b$  is the valence band. Hereafter, we focus on the  $\gamma^{-2}$ -term of  $\sigma_{xy}$ , which is given by  $(n_a, n_b) = (3, 0)$  terms shown in Fig. 2 and  $(n_a, n_b) = (3, 1)$  terms shown in Fig. 3. (Note that  $(n_a, n_b) = (4, 0)$  terms vanish identically, and the terms with  $n_a \leq 2$  give less divergent contribution.)

Thus, the exact expression for the most divergent  $\gamma^{-2}$ -term is obtained as

$$\begin{aligned}
\sigma_{xy} &= e^3 \frac{g_s}{2} \sum_{\mathbf{k}, a} \int \frac{d\epsilon}{2\pi} f'(\epsilon) \text{Im} \{ (G_a^{\text{R}})^2 G_a^{\text{A}} - G_a^{\text{R}} (G_a^{\text{A}})^2 \} \\
&\quad \times v_a^x [v_a^y v_a^{xy}(\epsilon) - v_a^x v_a^{yy}(\epsilon)] \quad (11) \\
&= -e^3 \frac{g_s}{2} \sum_{\mathbf{k}, a} f'(\epsilon_a) v_a^x [v_a^y v_a^{xy}(\epsilon_a) - v_a^x v_a^{yy}(\epsilon_a)] \frac{1}{2\gamma_a^2} \quad (12)
\end{aligned}$$

where we set  $\mu = y$  and  $\nu = x$  without loss of generality. In deriving Eq. (12), we used the relation  $i\{(G_a^{\text{R}})^2 G_a^{\text{A}} - G_a^{\text{R}} (G_a^{\text{A}})^2\} = \frac{\pi}{\gamma_a} \delta(\epsilon - \epsilon_a)$  [29, 55]. Here,

$$v_a^{\mu\nu}(\epsilon) = \bar{v}_a^{\mu\nu} + 2g_a^{\mu\nu}(\epsilon), \quad (13)$$

$$g_a^{\mu\nu}(\epsilon) = \frac{1}{2} \sum_{b \neq a} [v_{ab}^{\mu} v_{ba}^{\nu} + v_{ab}^{\nu} v_{ba}^{\mu}] \text{Re} G_b^{\text{R}}(\epsilon), \quad (14)$$

$$\text{Re} G_b(\epsilon) = \frac{\epsilon - \epsilon_b}{(\epsilon - \epsilon_b)^2 + \gamma_b^2}. \quad (15)$$

$g_a^{\mu\nu}(\epsilon)$  is called the qQM, which is significant in the presence of band-degeneracy, that is,  $\epsilon_{a,\mathbf{k}} \approx \epsilon_{b,\mathbf{k}}$  [56]. Importantly,  $g_a^{\mu\nu}(\epsilon)$  depends on the temperature through  $\gamma_b$ , which plays a crucial role in strongly correlated electron systems.

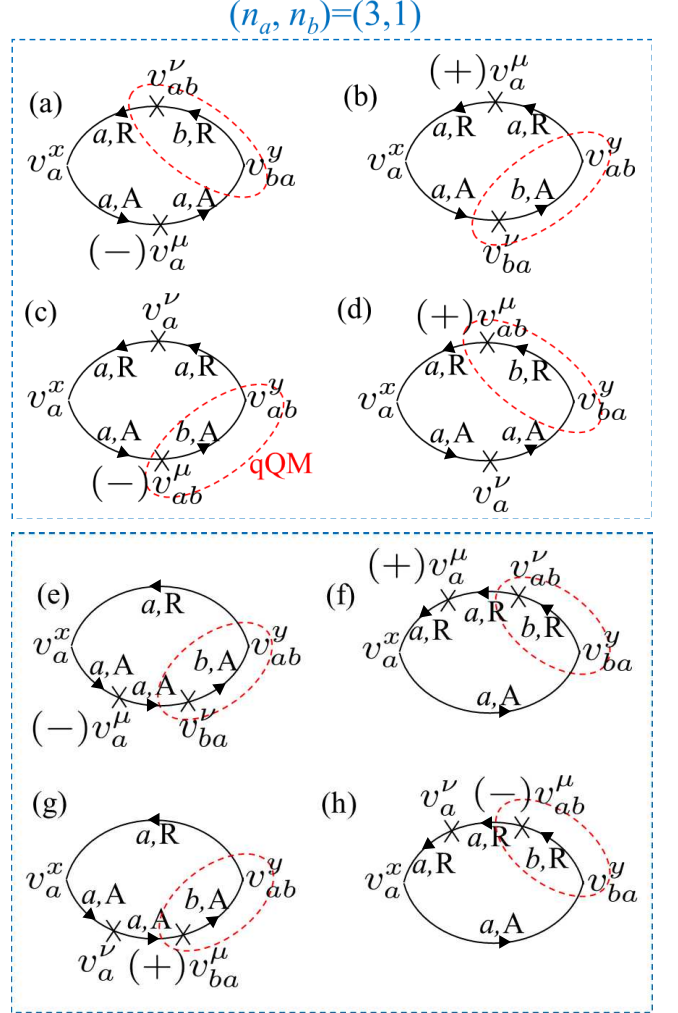


FIG. 3.  $(n_a, n_b) = (3, 1)$  terms for  $\sigma_{xy}$ , derived from the  $A_{\nu} q_{\mu}$ -linear terms from  $K(i\omega_l)$ .  $a$  ( $b$ ) represents the conduction (valence) band. The diagrams within the red dashed lines correspond to the qQM terms. We stress that (a)+(b)+(c)+(d) is equal to (e)+(f)+(g)+(h). Other  $(n_a, n_b) = (3, 1)$  terms are exactly canceled out.

When  $\gamma_b \ll |\epsilon_a - \epsilon_b|$ , the relation  $v_{a,\mathbf{k}}^{\mu\nu}(\epsilon_a) = \partial^{\mu} \partial^{\nu} \epsilon_{a,\mathbf{k}}$  is satisfied, which is derived from the kinetic equation without interactions. In this case, Eq. (12) reproduces the well-known relaxation-time approximation for single-band models. In contrast, when  $\gamma_b \gg |\epsilon_a - \epsilon_b|$ , the relation  $v_{a,\mathbf{k}}^{\mu\nu}(\epsilon_a) \approx \bar{v}_{a,\mathbf{k}}^{\mu\nu}$  is satisfied.

To summarize, we derived an rigorous formula of the normal Hall effect  $\sigma_{xy}$  in multiorbital tight-binding

model. The derived formula of  $\sigma_{xy}$  contains the qQM term, which exhibits prominent temperature dependence in strongly correlated metals. The present qQM mechanism causes the prominent  $T$ -dependence of  $R_H$  in bilayer nickelates. It is found that  $\sigma_{xy}$  exhibits the coherent-incoherent crossover, from  $\sigma_{xy}^{\text{coh}}$  [low- $\rho$  region] to  $\sigma_{xy}^{\text{incoh}}$  [high- $\rho$  region]. This is similar to the coherent-incoherent crossover of the anomalous Hall effect:  $\sigma_{\text{AHE}} \propto \text{const}$  for low- $\rho$  region and  $\sigma_{\text{AHE}} \propto \rho^{-2}$  for high- $\rho$  region [58].

In the presence of strong electron correlations, both the self-energy and the current vertex correction may play significant roles [29, 59]. As for the self-energy effect, the retarded Green function is given as  $G_a^R(\mathbf{k}, \epsilon) = (Z_a \epsilon - \tilde{\epsilon}_{a,\mathbf{k}} + i\gamma_a)^{-1}$ , where  $Z_a \equiv [(1 - \text{Re}(d\Sigma_a/d\epsilon)_{\epsilon=0})^{-1}]$  is the mass-enhancement factor and  $\tilde{\epsilon}_{a,\mathbf{k}} \equiv \epsilon_{a,\mathbf{k}} + \text{Re}\Sigma_{a,\mathbf{k}} - \mu$ . Considering the relation  $\delta(Z\epsilon - \epsilon_a) = Z^{-1}\delta(\epsilon - \epsilon_a/Z)$ , we can show that  $\sigma_{xy}$  given in Eq. (13) is independent of the factor  $Z_a$ . On the other hand, the current vertex corrections give rise to a prominent enhancement of the Hall conductivity and the magneto-conductivity [29]. The effect of the vertex correction for the qQM term would be a significant future problem.

### III. MODEL OF THIN-FILM $\text{La}_3\text{Ni}_2\text{O}_7$

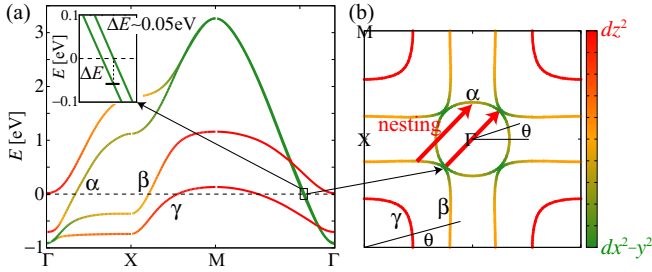


FIG. 4. (a) Band structure and (b) FSs for  $n = 2.6$  of thin-film  $\text{La}_3\text{Ni}_2\text{O}_7$ . The color bar indicates the orbital weight of  $d_{z^2}$ - and  $d_{x^2-y^2}$ -orbitals. The one-electron pocket is labeled by  $\alpha$ , and two hole pockets are labeled by  $\beta$ ,  $\gamma$ .  $\theta$  denotes the azimuthal angle from the  $x$ -axis. Red arrows represent the nesting vector.

Here, we construct the first-principles bilayer 2-orbital tight-binding model of thin-film  $\text{La}_3\text{Ni}_2\text{O}_7$ . We start with the bulk tight-binding model presented in previous work [54]. The model Hamiltonian consists of  $d_{z^2}$ - and  $d_{x^2-y^2}$ -orbitals for each upper and lower Ni layer. We denote the  $d_{z^2}$  and  $d_{x^2-y^2}$  orbitals in the upper (lower) layer as orbital  $l = 1(3)$  and  $l = 2(4)$ , respectively. To reproduce the band structure reported by ARPES measurement in thin-film  $\text{La}_3\text{Ni}_2\text{O}_7$  [5], we reduce the inter-layer hopping of  $d_{z^2}$ -orbital by 38%, shift the level of  $d_{z^2}$ -orbital by  $-0.45\text{eV}$ , and apply 20% hole doping to each Ni atom.

Figures 4 (a) and (b) show the band structure and Fermi surface (FS) in the present thin-film model for electron number  $n = 2.6$ , where the color bar indicates the

orbital component. There are three FSs labeled as  $\alpha$ ,  $\beta$ , and  $\gamma$ , where  $\alpha$ -pocket is an electron pocket around  $\Gamma$  point, and  $\beta$ ,  $\gamma$ -pockets are hole pockets around M point. The  $\alpha$ - and  $\beta$ -pockets are the mixture of two  $d$ -orbitals, while the  $\gamma$ -pocket is composed of the  $d_{z^2}$ -orbital. We also denote the bands including the  $\alpha$ ,  $\beta$ , and  $\gamma$  FSs as the  $\alpha$ ,  $\beta$ , and  $\gamma$  bands, respectively. Along the  $\Gamma$ -M line, the two  $d_{x^2-y^2}$ -orbital bands are nearly degenerate as shown in the inset of Fig. 4 (a), where the energy splitting  $\Delta E \sim 0.05\text{eV}$ . The origin of band degeneracy is attributed to the inter-layer hopping of the  $d_{x^2-y^2}$ -orbital mediated by  $s$ -orbital, as previously proposed in YBCO cuprates [60]. This inter-layer hopping is proportional to  $[\cos(k_x) - \cos(k_y)]^2$ . Since the inter-layer hopping vanishes along the  $\Gamma$ -M line,  $d_{x^2-y^2}$ -orbital bands on the two layers are nearly decoupled and degenerate.

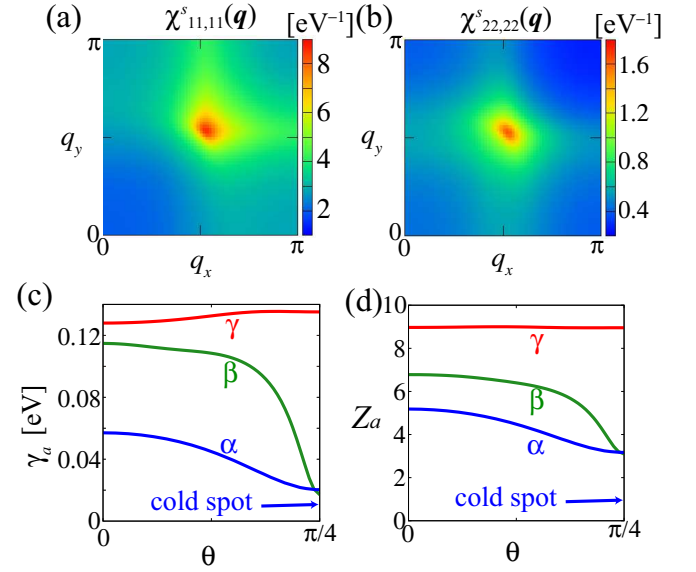


FIG. 5.  $\mathbf{q}$  dependences of (a)  $\chi_{11,11}^s(\mathbf{q})$  and (b)  $\chi_{22,22}^s(\mathbf{q})$  for  $U = 2.74\text{eV}$ ,  $J/U = 0.2$  ( $\alpha_s = 0.97$  at  $T = 10\text{meV}$ ) in the FLEX approximation.  $\theta$  dependences of (c) damping  $\gamma_a$  and (d) mass enhancement  $Z_a$  on the FSs in the band representation for  $U = 2.74\text{eV}$ ,  $J/U = 0.2$  at  $T = 10\text{meV}$ .

### IV. THE RESULTS OF FLEX AND RESISTIVITY

Here, we analyze the self-energy  $\hat{\Sigma}$  in the fluctuation-exchange (FLEX) approximation. Details of formulation are explained in Appendix A. In the FLEX approximation, the spin susceptibilities are dominant over the charge susceptibilities. Since the vertex corrections are not taken into account in the FLEX approximation, the charge susceptibilities are underestimated. Figures 5 (a) and (b) show the obtained intra-layer spin susceptibilities  $\chi_{11,11}^s(\mathbf{q}, 0)$  and  $\chi_{22,22}^s(\mathbf{q}, 0)$  for  $U = 2.74\text{eV}$ ,  $J/U = 0.2$  at  $T = 10\text{meV}$  in the FLEX approximation,



where the Stoner factor is  $\alpha_s = 0.97$ .  $\chi_{11,11}^s (= \chi_{33,33}^s)$  is dominant over  $\chi_{22,22}^s (= \chi_{44,44}^s)$  and takes large values at  $\mathbf{q} \sim (\pi/2, \pi/2)$ . This peak position corresponds to the nesting vector shown in Fig. 4 (b). The inter-layer susceptibility  $\chi_{11,33}^s$  (not shown) is negative and a little smaller than  $\chi_{11,11}^s$ . Similar results have been reported in bulk  $\text{La}_3\text{Ni}_2\text{O}_7$  [33, 61, 62]. Figures 5 (c) and (d) show the obtained  $\theta$  dependence of damping  $\gamma_a \equiv -\text{Im}\Sigma_a^R$  and mass-enhancement factor  $Z_a \equiv 1 - \text{Re}\frac{\partial\Sigma_a^R(\epsilon)}{\partial\epsilon}|_{\epsilon=0}$  on the FSs in the band representation for  $U = 2.74\text{eV}$ ,  $J/U = 0.2$  at  $T = 10\text{meV}$ ,  $\theta$  denotes the azimuthal angle from the  $x$ -axis. The behaviors of  $\gamma_a$  and  $Z_a$  are similar. The  $\alpha$  and  $\beta$  FSs become the cold spots at  $\theta = \pi/4$ , where the weight of the  $d_{x^2-y^2}$  orbital is dominant, since the value of  $\chi_{22,22}^s$  is much smaller than  $\chi_{11,11}^s$ . Thus, the orbital-selective cold spots emerge in  $\text{La}_3\text{Ni}_2\text{O}_7$ .

Using the self-energy in the FLEX approximation, transport phenomena are analyzed by the linear response theory. We calculate  $\rho$ ,  $R_H$ , Nernst coefficient  $\nu$ , and the Seebeck coefficient  $S$  in the band representation. Details of the formulation are explained in Appendix A. Figure 6 (a) exhibits  $T$ -dependences of  $\rho$  for  $J/U = 0.25, 0.2$ , and  $0.15$ , where  $\alpha_s = 0.95$  is satisfied at  $T = 10\text{meV}$ . Non-Fermi-liquid behavior  $\rho \propto T$  is obtained due to the strong spin fluctuations. The origin of the  $T$  dependence is  $\gamma \propto T$  around the cold spots as shown in Fig. 6 (b). This result is consistent with the experimental results [1, 4]. Non-Fermi-liquid behavior  $\rho \propto T$  has also been obtained in other strongly correlated electron systems.

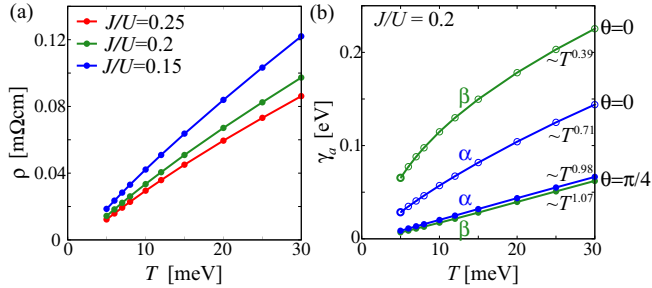


FIG. 6. (a)  $T$  dependences of  $\rho$  for  $J/U = 0.25, 0.2, 0.15$ , where  $\alpha_s = 0.95$  is satisfied at  $T = 10\text{meV}$ . (b)  $T$  dependences of  $\gamma_a$  for  $\theta = 0, \pi/4$  on  $\alpha$  and  $\beta$  FSs for  $U = 2.74\text{eV}$ ,  $J/U = 0.2$ .

## V. RESULTS OF HALL COEFFICIENT AND NERNST COEFFICIENT

Here, we analyze the transport coefficient using the novel formula that incorporates the qQM term  $g_a^{\mu\nu}[\gamma]$ . This qQM term, which fully captures many-body effects by accounting for the  $T$  dependence of  $\gamma$ , plays a crucial role in determining  $R_H$  and  $\nu$ .  $g_a^{\mu\nu}$  term in Eq. (14) is composed of the inter-band terms such as  $v_{ab}^\mu$ . As shown in Sec. II, the result of the conventional RTA is reproduced by using  $g_a^{\mu\nu}[0]$ . On the other hand, the result

given by using  $g_a^{\mu\nu}[\infty] = 0$  corresponds to the single-band approximation, where the qQM term is absent. In the following, we denote the Hall coefficients obtained by using  $g_a^{\mu\nu}[\gamma]$ ,  $g_a^{\mu\nu}[0]$ , and  $g_a^{\mu\nu}[\infty]$  as  $R_H$ ,  $R_H^{\text{RTA}}$ , and  $R_H^{\text{no qQM}}$ , respectively. We also denote the Nernst coefficients obtained by using  $g_a^{\mu\nu}[\gamma]$ ,  $g_a^{\mu\nu}[0]$ , and  $g_a^{\mu\nu}[\infty]$  as  $\nu$ ,  $\nu^{\text{RTA}}$ , and  $\nu^{\text{no qQM}}$ , respectively.

Figure 7 shows  $\theta$  dependences of  $g_a^{\mu\nu}[\gamma]$ ,  $g_a^{\mu\nu}[0]$ , and  $\bar{v}_a^{\mu\nu}$  on FSs ( $\epsilon = \mu$ ) for  $U = 2.74\text{eV}$ ,  $J/U = 0.2$  at  $T = 5\text{meV}$ . The value of  $g_a^{\mu\nu}[\gamma]$  at cold spot ( $\theta = \pi/4$ ) is close to that of  $g_a^{\mu\nu}[0]$  and significantly larger than that of  $\bar{v}_a^{\mu\nu}$  at low temperatures. This behavior arises from the qQM terms, which are enhanced when  $\gamma$  and  $\mu - \epsilon_b$  are small, as indicated by the expression of  $\text{Re}G$  in Eq. (15). In  $\text{La}_3\text{Ni}_2\text{O}_7$ , the relation  $\Delta E = \mu - \epsilon_b \sim 0.05\text{eV}$  at the cold spots is intrinsically satisfied since the two  $d_{x^2-y^2}$  bands are nearly degenerate along  $\Gamma$ -M line as shown in Fig. 4 (a).

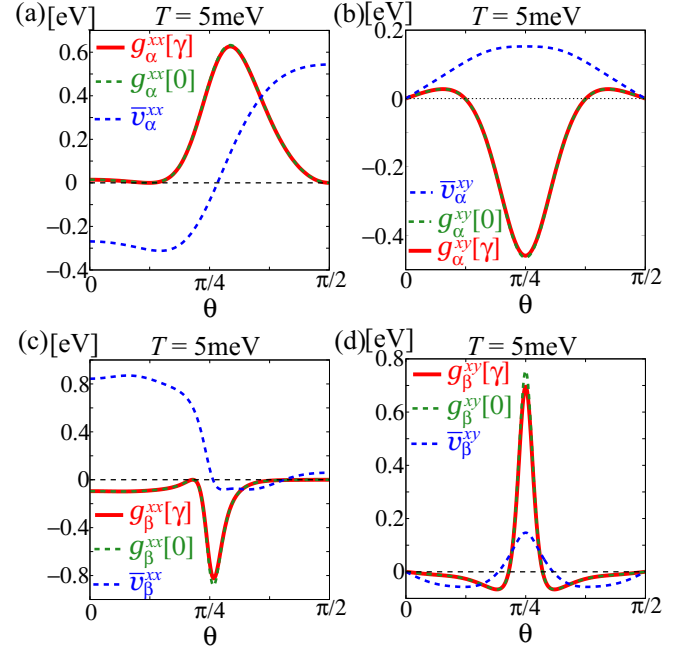


FIG. 7.  $\theta$  dependences of (a)  $g_\alpha^{xx}[\gamma]$ ,  $g_\alpha^{xx}[0]$ , and  $\bar{v}_\alpha^{xx}$ , (b)  $g_\alpha^{xy}[\gamma]$ ,  $g_\alpha^{xy}[0]$ , and  $\bar{v}_\alpha^{xy}$ , (c)  $g_\beta^{xx}[\gamma]$ ,  $g_\beta^{xx}[0]$ , and  $\bar{v}_\beta^{xx}$ , and (d)  $g_\beta^{xy}[\gamma]$ ,  $g_\beta^{xy}[0]$ , and  $\bar{v}_\beta^{xy}$  on FSs ( $\epsilon = \mu$ ) for  $U = 2.74\text{eV}$ ,  $J/U = 0.2$  at  $T = 5\text{meV}$ .  $\theta = \pi/4$  corresponds to the cold spot.

Figure 8 (a) shows  $T$  dependences of  $R_H$ ,  $R_H^{\text{RTA}}$ , and  $R_H^{\text{no qQM}}$  for  $U = 2.74\text{eV}$ ,  $J/U = 0.2$ . The experimental results reported in Ref. [1] are also included for comparison. The values of  $R_H$  and  $R_H^{\text{RTA}}$  at low  $T$  are much larger than that of  $R_H^{\text{no qQM}}$ , which means that the qQM terms are important for  $R_H$  including the second derivative velocity  $v^{\mu\nu}$ . As shown in Fig. 6 (b), the relation  $\gamma \sim \Delta E$  ( $\sim 0.05\text{eV}$ ) is satisfied at  $T = T_{\text{coh}} \sim 23\text{meV}$ . For  $T < T_{\text{coh}}$ ,  $R_H$  is close to  $R_H^{\text{RTA}}$  due to  $\gamma < \Delta E$ . In contrast, for  $T > T_{\text{coh}}$ ,  $\gamma$  becomes large ( $\gamma > \Delta E$ ), and  $R_H$  is close to  $R_H^{\text{no qQM}}$ . Thus, around  $T \sim T_{\text{coh}}$   $R_H$

crossovers from  $R_H^{\text{RTA}}$  with small  $\gamma$  (coherent regime) to  $R_H^{\text{no qQM}}$  with large  $\gamma$  (incoherent regime). Due to this coherent-incoherent crossover behavior, discussed in Sec. II, the  $T$  dependence of  $R_H$  is more significant than that of  $R_H^{\text{RTA}}$ . Notably, the obtained  $T$  dependence of  $R_H$  is consistent with experimental results in thin-film bilayer nickelates [1, 4].

Figures 8 (b) and (c) show  $\mathbf{k}$  dependences of  $\sigma_{xy}(\mathbf{k})$ , where  $\sigma_{xy}$  is given by  $\sigma_{xy} = \frac{1}{N} \sum_{\mathbf{k}} \sigma_{xy}(\mathbf{k})$ . These results indicate that the dominant contributions to  $R_H$  originate from the cold spots. The hole pocket  $\beta$  contributes positively to  $R_H$ , whereas the electron pocket  $\alpha$  contributes negatively to  $R_H$ . Competition between the contributions from  $\alpha$  and  $\beta$  pockets is important to determine both the sign and  $T$  dependence of  $R_H$ . At low  $T$ , the contribution from the vicinity of the FS at cold spots is dominant. Furthermore,  $\gamma$  on hole pocket  $\beta$  at cold spots is smaller than that on electron pocket  $\alpha$ , as shown in Fig. 5 (c). In this case, the positive contribution is dominant over the negative one, as shown in Fig. 8 (b). In contrast, at high  $T$ , the contributions from the two pockets are comparable since the negative contribution from the  $\alpha$  pocket relatively develops away from the cold spots, as shown in Fig. 8 (c).

Figure 8 (d) exhibits  $T$  dependences of  $\nu$ ,  $\nu^{\text{RTA}}$ , and  $\nu^{\text{no qQM}}$  for  $U = 2.74\text{eV}$ ,  $J/U = 0.2$ . At low  $T$ ,  $\nu$  and  $\nu^{\text{RTA}}$  are significantly larger in magnitude than  $\nu^{\text{no qQM}}$ , which also means that the qQM terms are important for  $\nu$  including the second derivative velocity  $v^{\mu\nu}$ . In contrast to  $R_H$ ,  $\nu$  is negative, which decreases at low  $T$ .  $\nu$  is close to  $\nu^{\text{RTA}}$  for  $T < T_{\text{coh}}$ , while  $\nu$  is close to  $\nu^{\text{no qQM}}$  for  $T > T_{\text{coh}}$ . This coherent-incoherent crossover behavior is similar to that of  $R_H$ .

## VI. DISCUSSION

Here, we discuss the competing contributions to transport phenomena from the  $\alpha$  and the  $\beta$  bands. Figures 9 (a) and (b) show the contributions to  $\sigma_{xy}/B$  and  $\alpha_{xy}/B$  from  $\alpha$  and  $\beta$  bands obtained by using  $g_a^{\mu\nu}[\gamma]$  for  $U = 2.74\text{eV}$ ,  $J/U = 0.2$ . We find that the positive contribution from  $\beta$  band to  $\sigma_{xy}$  strongly competes with the negative one from  $\alpha$  band. Thus, the sign of  $R_H$  is sensitive to the parameters such as  $U$  and  $J$ , as shown in Fig. 10 (a) in Appendix B. In contrast, the almost perfect cancellation of the  $\alpha$  and  $\beta$  bands in  $\sigma_{xy}$  does not exist in  $\alpha_{xy}$ . Therefore, negative  $\alpha_{xy}$  and  $\nu$ , mainly given by  $\alpha$  band, are greatly enhanced at low temperatures. These behaviors are robust against the value of  $U$  as shown in Fig. 11 in Appendix B. The possible reasons for incomplete cancellation in  $\alpha_{xy}$  are (i) asymmetry with respect to energy  $\epsilon$  in  $\gamma_a$  and (ii) contributions away from the cold spots are different between  $\alpha$  and  $\beta$  bands.

We also calculate Seebeck coefficient  $S$  as shown in Fig. 12 in Appendix B. The obtained  $S$  is negative and increases with decreasing  $T$ , which is similar to the behavior observed in triple-layer and quintuple-layer nick-

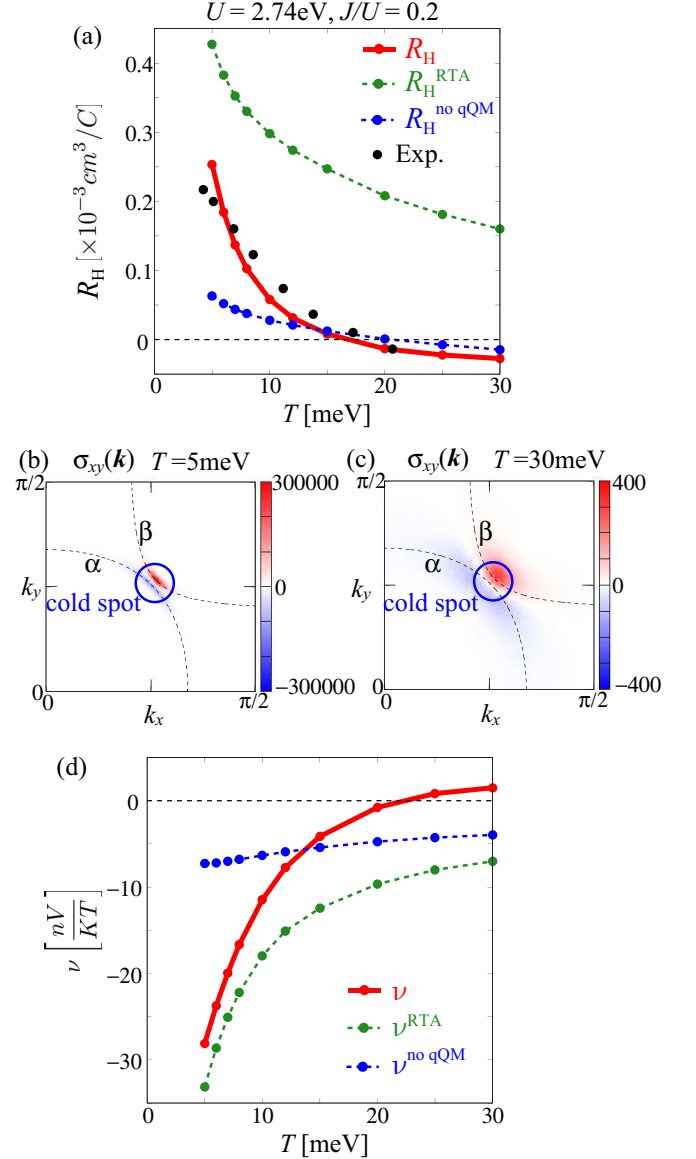


FIG. 8. (a)  $T$  dependences of  $R_H$ ,  $R_H^{\text{RTA}}$ , and  $R_H^{\text{no qQM}}$  for  $U = 2.74\text{eV}$ ,  $J/U = 0.2$ . The experimental results reported in Ref. [1] are plotted as black dots.  $\mathbf{k}$  dependences of  $\sigma_{xy}(\mathbf{k})$  obtained by using  $g_a^{\mu\nu}[\gamma]$  at (b)  $T = 5\text{meV}$  and (c)  $T = 30\text{meV}$  for  $U = 2.74\text{eV}$ ,  $J/U = 0.2$ . Dashed lines represent FSs. Blue circles represent cold spots. (d)  $T$  dependences of  $\nu$ ,  $\nu^{\text{RTA}}$ , and  $\nu^{\text{no qQM}}$  for  $U = 2.74\text{eV}$ ,  $J/U = 0.2$ .

elates [63].

Here, we note that the transport phenomena are not affected qualitatively by the CDW fluctuations. Since the  $d_{x^2-y^2}$ -orbital component in the CDW fluctuations is dominant and  $\mathbf{q}$  dependence is similar to the SDW fluctuations [54], the contribution from the CDW fluctuations to  $d_{x^2-y^2}$ -orbital cold spots is expected to be small. Thus, the CDW fluctuations are expected to make no qualitative difference for the transport phenomena. In the present study, we ignore the CDW fluctuations and the CVC for simplicity.

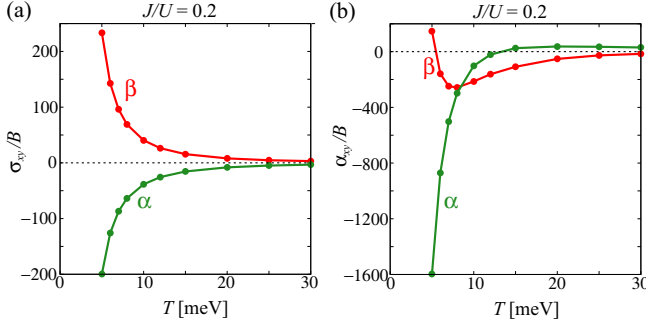


FIG. 9.  $T$  dependences of (a)  $\sigma_{xy}/B$  and (b)  $\alpha_{xy}/B$  for  $\alpha$  and  $\beta$  bands obtained by using  $g_a^{\mu\nu}[\gamma]$  for  $U = 2.74\text{eV}$  with  $J/U = 0.2$ .

## VII. SUMMARY

In this paper, we studied the origin of non-Fermi-liquid transport phenomena in thin-film bilayer nickelate  $\text{La}_3\text{Ni}_2\text{O}_7$ . We derived a novel formula for the  $R_H$  that incorporates the important many-body effects within the qQM term. The  $T$  dependence of the quasi-particle damping  $\gamma$  is introduced into the qQM term in the formula. We discovered that the qQM term becomes significant inevitably in  $\text{La}_3\text{Ni}_2\text{O}_7$ , owing to the band degeneracy at the orbital-selective cold spots. The obtained  $\rho \propto T$  and positive  $R_H$  increasing at low  $T$  are consistent with experiments. The qQM term is also essential for the Nernst coefficient and other transport phenomena involving the second derivative velocity  $v^{\mu\nu}$ .  $\text{La}_3\text{Ni}_2\text{O}_7$  is a promising platform for exploring the physics of the qQM.

## ACKNOWLEDGMENTS

We are grateful to Y. Nomura and M. Osada for fruitful discussions. This work was supported by JSPS KAKENHI Grant Numbers JP25H01246, JP25H01248, JP24K00568, JP24K06938, JP23K03299, JP22K14003.

### A. Appendix A: Formulation of FLEX and transport phenomena

The self-energy in the FLEX approximation  $\hat{\Sigma}$ , the effective interaction for the self-energy in the FLEX approximation  $\hat{V}$ , the spin (charge) susceptibility  $\hat{\chi}^{s(c)}$ , the irreducible susceptibility  $\hat{\chi}^0$ , and Green's function  $\hat{G}$  are given as

$$\Sigma_{lm}(k) = \frac{T}{N} \sum_q V_{ll',mm'}(q) G_{l'm'}(k-q), \quad (16)$$

$$\hat{V}(q) = \frac{3}{2} \hat{\Gamma}^s \hat{\chi}^s(q) \hat{\Gamma}^s + \frac{1}{2} \hat{\Gamma}^c \hat{\chi}^c(q) \hat{\Gamma}^c$$

$$-\frac{1}{2} [\hat{\Gamma}^c \hat{\chi}^0(q) \hat{\Gamma}^c + \hat{\Gamma}^s \hat{\chi}^0(q) \hat{\Gamma}^s - \frac{1}{4} (\hat{\Gamma}^s + \hat{\Gamma}^c) \hat{\chi}^0(q) (\hat{\Gamma}^s + \hat{\Gamma}^c)], \quad (17)$$

$$\hat{\chi}^{s(c)}(q) = \frac{\hat{\chi}^0(q)}{1 - \hat{\Gamma}^{s(c)} \hat{\chi}^0(q)}, \quad (18)$$

$$\chi_{ll',mm'}^0(q) = -\frac{T}{N} \sum_k G_{lm}(k+q) G_{m'l'}(k), \quad (19)$$

$$\hat{G}(k) = \left[ \frac{1}{i\epsilon_n \hat{1} - \hat{h}_{\mathbf{k}} - \hat{\Sigma}(k)} \right], \quad (20)$$

where  $k = [\mathbf{k}, \epsilon_n = (2n+1)\pi T]$ ,  $q = (\mathbf{q}, \omega_m = 2m\pi T)$ . We put the chemical potential  $\mu = 0$ . The on-site bare Coulomb interaction  $\hat{\Gamma}^s$  for the spin channel on the upper layer ( $l_1, l_2, l_3, l_4 = 1, 2$ ) or the lower layer ( $l_1, l_2, l_3, l_4 = 3, 4$ ) is given as

$$(\Gamma^s)_{l_1 l_2, l_3 l_4} = \begin{cases} U, & l_1 = l_2 = l_3 = l_4 \\ U', & l_1 = l_3 \neq l_2 = l_4 \\ J, & l_1 = l_2 \neq l_3 = l_4 \\ J, & l_1 = l_4 \neq l_2 = l_3 \\ 0, & \text{otherwise,} \end{cases} \quad (21)$$

where the inter-orbital Coulomb interaction  $U' = U - 2J$ . Also, the on-site bare Coulomb interaction  $\hat{\Gamma}^c$  for the charge channel is given as

$$(\hat{\Gamma}^c)_{l_1 l_2, l_3 l_4} = \begin{cases} -U, & l_1 = l_2 = l_3 = l_4 \\ U' - 2J, & l_1 = l_3 \neq l_2 = l_4 \\ -2U' + J, & l_1 = l_2 \neq l_3 = l_4 \\ -J, & l_1 = l_4 \neq l_2 = l_3 \\ 0, & \text{otherwise.} \end{cases} \quad (22)$$

In the present 3D calculation, we employ  $N = 128 \times 128$   $\mathbf{k}(\mathbf{q})$  meshes and 512 Matsubara frequencies.  $\hat{h}_{\mathbf{k}}$  is the matrix expression of the Hamiltonian  $H$ .

To obtain the real frequency dependence, we use the analytic continuation by the Pade approximation,

$$\hat{\Sigma}(\mathbf{k}, i\epsilon_n) \rightarrow \hat{\Sigma}_{\mathbf{k}}^R(\epsilon), \quad (23)$$

$$\hat{G}_{\mathbf{k}}^R(\epsilon) = \left[ \frac{1}{\epsilon \hat{1} - \hat{h}_{\mathbf{k}} - \hat{\Sigma}_{\mathbf{k}}^R(\epsilon)} \right]. \quad (24)$$

The conductivity  $\sigma_{xx}$  is given as,

$$\sigma_{xx} = e^2 \sum_{\mathbf{k}, a} \int \frac{d\epsilon}{\pi} \left( -\frac{\partial f}{\partial \epsilon} \right) \times v_a^x G_a^R v_a^x G_a^A, \quad (25)$$

where  $f(\epsilon) = [\exp(\epsilon/T) + 1]^{-1}$ , and  $-e$  ( $e > 0$ ) is the electron charge. The velocity is given as  $v_{a,\mathbf{k}}^x = \frac{\partial \epsilon_{a,\mathbf{k}}}{\partial k_x}$ , and the resistivity along  $x$ -axis is given as,

$$\rho = \frac{1}{\sigma_{xx}}. \quad (26)$$

The Seebeck coefficient  $S$  is given by

$$S = -e \frac{\alpha_{xx}}{T \sigma_{xx}}, \quad (27)$$

$$\alpha_{xx} = \sum_{\mathbf{k}, a} \int \frac{d\epsilon}{\pi} \left( -\frac{\partial f}{\partial \epsilon} \right) \epsilon \times v_a^x G_a^R v_a^x G_a^A. \quad (28)$$

The Nernst coefficient  $\nu$  is given by

$$\nu = \frac{\alpha_{xy}}{B \sigma_{xx}} - \frac{S \sigma_{xy}}{B \sigma_{xx}}, \quad (29)$$

$$\begin{aligned} \alpha_{xy} &= B \frac{e^2}{T} \sum_{\mathbf{k}, a} \int \frac{d\epsilon}{\pi} f'(\epsilon) \epsilon |\text{Im} G_a^R| |G_a^R|^2 \\ &\quad \times v_a^x [v_a^y v_a^{xy}(\epsilon) - v_a^x v_a^{yy}(\epsilon)] \\ &= B \frac{e^2}{T} \sum_{\mathbf{k}, a} f'(\epsilon_a) \epsilon_a v_a^x [v_a^y v_a^{xy}(\epsilon_a) - v_a^x v_a^{yy}(\epsilon_a)] \frac{1}{2\gamma_a^2} \end{aligned} \quad (30)$$

In order to convert the unit of transport coefficients to the experimental unit, we use lattice constant  $a = b = 3.715\text{\AA}$ ,  $c = 19.7\text{\AA}$ .

## B. Appendix B: Additional results of transport phenomena

Figures 10 (a) and (b) exhibit  $T$  dependences of  $R_H$  and  $\nu$  for  $U = 1.82\text{eV}$ ,  $J/U = 0.2$ . Here,  $\alpha_s = 0.93$  is satisfied at  $T = 10\text{meV}$ . In this case,  $R_H$  and  $\nu$  are negative at low  $T$ . The  $T$  dependence of  $R_H$  is sensitive to the competition between the contributions from  $\alpha$  and  $\beta$  pockets, whereas the negative  $\nu$  decreasing at low  $T$  is robust in the thin-film  $\text{La}_3\text{Ni}_2\text{O}_7$  model. We find that  $R_H$  becomes negative in the regime of weak electronic correlations, i.e., when the values of  $U$  and  $J$  are small.  $R_H$  and  $\nu$  are closer to  $R_H^{\text{RTA}}$  and  $\nu^{\text{RTA}}$  than Figs. 8 (a) and (d) for  $U = 2.74\text{eV}$  since  $\gamma$  for  $U = 1.82\text{eV}$  is smaller than that for  $U = 2.74\text{eV}$ .

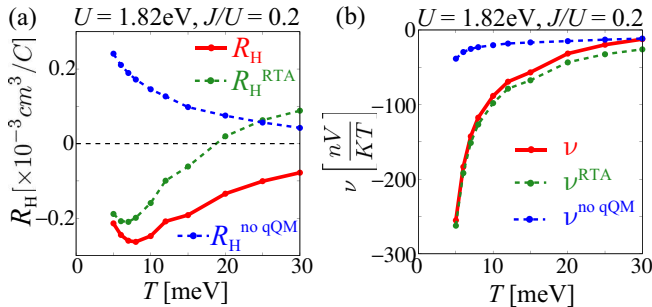


FIG. 10. (a)  $T$  dependences of  $R_H$ ,  $R_H^{\text{RTA}}$ , and  $R_H^{\text{no qQM}}$  for  $U = 1.82\text{eV}$ ,  $J/U = 0.2$  ( $\alpha_s = 0.93$  at  $T = 10\text{meV}$ ), and (b) Those of  $\nu$ ,  $\nu^{\text{RTA}}$ , and  $\nu^{\text{no qQM}}$

Figures 11 (a) and (b) show the contributions of  $\sigma_{xy}/B$  and  $\alpha_{xy}/B$  from  $\alpha$  and  $\beta$  bands given by using  $g_a^{\mu\nu}[\gamma]$  for  $U = 1.82\text{eV}$ ,  $J/U = 0.2$ . These behaviors are similar to those for  $U = 1.82\text{eV}$ ,  $J/U = 0.2$  in Figs. 9(a) and (b).

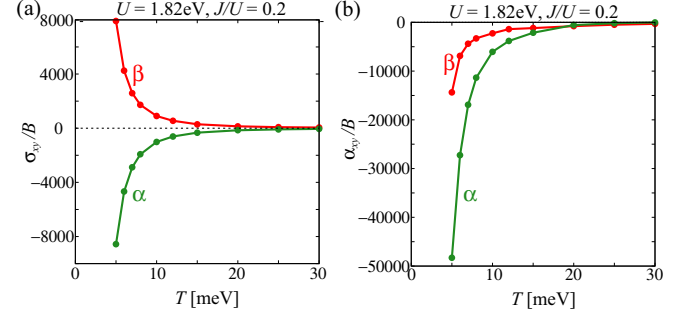


FIG. 11.  $T$  dependences of (a)  $\sigma_{xy}/B$  and (b)  $\alpha_{xy}/B$  for  $\alpha$  and  $\beta$  bands given by using  $g_a^{\mu\nu}[\gamma]$  for  $U = 1.82\text{eV}$  with  $J/U = 0.2$ .

Figure 12 shows  $T$  dependences of  $S$  for  $U = 2.74\text{eV}$  and  $U = 1.82\text{eV}$  at  $J/U = 0.2$ . The obtained  $S$  is negative and increases with decreasing  $T$ , which is similar to the behavior observed in triple-layer and quintuple-layer nickelates [63].

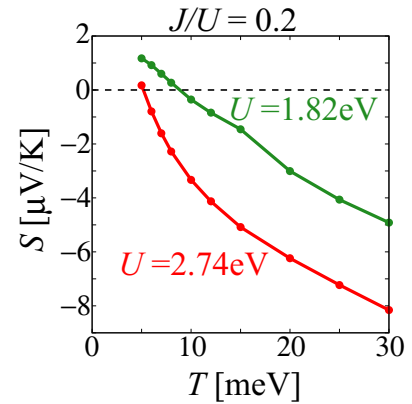


FIG. 12.  $T$  dependences of Seebeck coefficient  $S$  for  $U = 2.74\text{eV}$  and  $1.82\text{eV}$  at  $J/U = 0.2$ .



- 
- [1] E. K. Ko, Y. Yu, Y. Liu, L. Bhatt, J. Li, V. Thampy, C.-T. Kuo, B. Y. Wang, Y. Lee, K. Lee, J.-S. Lee, B. H. Goodge, D. A. Muller, and H. Y. Hwang, Signatures of ambient pressure superconductivity in thin film  $\text{La}_3\text{Ni}_2\text{O}_7$ , *Nature* **638**, 935 (2025).
- [2] G. Zhou, W. Lv, H. Wang, Z. Nie, Y. Chen, Y. Li, H. Huang, W. Chen, Y. Sun, Q.-K. Xue, Z. Chen, Ambient-pressure superconductivity onset above 40 K in bilayer nickelate ultrathin films, *Nature* **640**, 641 (2025).
- [3] M. Osada, C. Terakura, A. Kikkawa, M. Nakajima, H.-Y. Chen, Y. Nomura, Y. Tokura, and A. Tsukazaki, Strain-tuning for superconductivity in  $\text{La}_3\text{Ni}_2\text{O}_7$  thin films, *Commun. Phys.* **8**, 251 (2025).
- [4] Y.-T. Hsu, Y. Liu, Y. Kohama, T. Kotte, V. Sharma, Y. Tarn, Y. Yu, and H. Y. Hwang, Fermi-liquid transport beyond the upper critical field in superconducting  $\text{La}_2\text{PrNi}_2\text{O}_7$  thin films, *arXiv:2505.19011*.
- [5] P. Li *et al.*, Photoemission evidence for multi-orbital hole-doping in superconducting  $\text{La}_{2.85}\text{Pr}_{0.15}\text{Ni}_2\text{O}_7/\text{SrLaAlO}_4$  interfaces, *Natl. Sci. Rev.* **nwaf205** (2025).
- [6] H. Sun, M. Huo, X. Hu, J. Li, Z. Liu, Y. Han, L. Tang, Z. Mao, P. Yang, B. Wang, J. Cheng, D.-X. Yao, G.-M. Zhang, and M. Wang, Signatures of superconductivity near 80 K in a nickelate under high pressure, *Nature* **621**, 493 (2023).
- [7] G. Wang, N. N. Wang, X. L. Shen, J. Hou, L. Ma, L. F. Shi, Z. A. Ren, Y. D. Gu, H. M. Ma, P. T. Yang, Z. Y. Liu, H. Z. Guo, J. P. Sun, G. M. Zhang, S. Calder, J.-Q. Yan, B. S. Wang, Y. Uwatoko, and J.-G. Cheng, Pressure-Induced Superconductivity In Polycrystalline  $\text{La}_3\text{Ni}_2\text{O}_{7-\delta}$ , *Phys. Rev. X* **14**, 011040 (2024).
- [8] Y. Zhang, D. Su, Y. Huang, Z. Shan, H. Sun, M. Huo, K. Ye, J. Zhang, Z. Yang, Y. Xu, Y. Su, R. Li, M. Smidman, M. Wang, L. Jiao, and H. Yuan, High-temperature superconductivity with zero resistance and strange-metal behaviour in  $\text{La}_3\text{Ni}_2\text{O}_{7-\delta}$ , *Nat. Phys.* **20**, 1269 (2024).
- [9] Z. Dan, Y. Zhou, M. Huo, Y. Wang, L. Nie, M. Wang, T. Wu, and X. Chen, Pressure-enhanced spin-density-wave transition in double-layer nickelate  $\text{La}_3\text{Ni}_2\text{O}_{7-\delta}$ , *Sci. Bull.* **70**, 1239 (2025).
- [10] M. Kakoi, T. Oi, Y. Ohshita, M. Yashima, K. Kuroki, T. Kato, H. Takahashi, S. Ishiwata, Y. Adachi, N. Hatada, T. Uda, and H. Mukuda, Multiband Metallic Ground State in Multilayered Nickelates  $\text{La}_3\text{Ni}_2\text{O}_7$  and  $\text{La}_4\text{Ni}_3\text{O}_{10}$  Probed by  $^{139}\text{La}$ -NMR at Ambient Pressure, *J. Phys. Soc. Jpn.* **93**, 053702 (2024).
- [11] K. Chen, X. Liu, J. Jiao, M. Zou, C. Jiang, X. Li, Y. Luo, Q. Wu, N. Zhang, Y. Guo, and L. Shu, Evidence of Spin Density Waves in  $\text{La}_3\text{Ni}_2\text{O}_{7-\delta}$ , *Phys. Rev. Lett.* **132**, 256503 (2024).
- [12] R. Khasanov, Thomas J. Hicken, D. J. Gawryluk, Loïc P. Sorel, S. Bötzel, F. Lechermann, I. M. Eremin, H. Luetkens, and Z. Guguchia, Pressure-enhanced splitting of the density wave transitions in  $\text{La}_3\text{Ni}_2\text{O}_{7-\delta}$ , *Nat. Phys.* **21**, 430 (2025).
- [13] X. Chen, J. Choi, Z. Jiang, J. Mei, K. Jiang, J. Li, S. Agrestini, M. Garcia-Fernandez, X. Huang, H. Sun, D. Shen, M. Wang, J. Hu, Y. Lu, K.-J. Zhou, and D. Feng, Electronic and magnetic excitations in  $\text{La}_3\text{Ni}_2\text{O}_7$ , *Nat. Commun.* **15**, 9597 (2024).
- [14] N. K Gupta, R. Gong, Y. Wu, M. Kang, C. T. Parzyck, B. Z. Gregory, N. Costa, R. Sutarto, S. Sarker, A. Singer, D. G. Schlom, K. M. Shen, and D. G. Hawthorn, Anisotropic Spin Stripe Domains in Bilayer  $\text{La}_3\text{Ni}_2\text{O}_7$ , *arXiv:2409.03210* (2024).
- [15] X. Ren, R. Sutarto, X. Wu, J. Zhang, H. Huang, T. Xiang, J. Hu, R. Comin, X. J. Zhou, and Z. Zhu, Resolving the Electronic Ground State of  $\text{La}_3\text{Ni}_2\text{O}_{7-\delta}$  Films, *Commun. Phys.* **8**, 52 (2025).
- [16] J. Luo, J. Feng, G. Wang, N. N. Wang, J. Dou, A. F. Fang, J. Yang, J. G. Cheng, Guo-qing Zheng, and R. Zhou, Microscopic evidence of charge- and spin-density waves in  $\text{La}_3\text{Ni}_2\text{O}_{7-\delta}$  revealed by  $^{139}\text{La}$ -NQR, *Chin. Phys. Lett.* **42**, 067402 (2025).
- [17] T. Xie, M. Huo, X. Ni, F. Shen, X. Huang, H. Sun, H. C. Walker, D. Adroja, D. Yu, B. Shen, L. He, K. Cao, and M. Wang, Strong interlayer magnetic exchange coupling in  $\text{La}_3\text{Ni}_2\text{O}_{7-\delta}$  revealed by inelastic neutron scattering, *Sci. Bull.* **69**, 3221 (2024).
- [18] Z. Liu, H. Sun, M. Huo, X. Ma, Y. Ji, L. Li, H. Liu, J. Yu, Z. Zhang, Z. Chen, F. Liang, H. Dong, H. Guo, D. Zhong, B. Shen, S. Li, and M. Wang, Evidence for charge and spin density waves in single crystals of  $\text{La}_3\text{Ni}_2\text{O}_7$  and  $\text{La}_3\text{Ni}_2\text{O}_6$ , *Sci. China Phys. Mech. Astron.* **66**, 217411 (2022).
- [19] G. Wu, J. J. Neumeier, and M. F. Hundley, Magnetic susceptibility, heat capacity, and pressure dependence of the electrical resistivity of  $\text{La}_3\text{Ni}_2\text{O}_7$  and  $\text{La}_4\text{Ni}_3\text{O}_{10}$ , *Phys. Rev. B* **63**, 245120 (2001).
- [20] D. Li, B. Y. Wang, K. Lee, S. P. Harvey, M. Osada, B. H. Goodge, L. F. Kourkoutis, and H. Y. Hwang, Superconducting Dome in  $\text{Nd}_{1-x}\text{Sr}_x\text{NiO}_2$  Infinite Layer Films, *Phys. Rev. Lett.* **125**, 027001 (2020).
- [21] N. N. Wang, M. W. Yang, Z. Yang, K. Y. Chen, H. Zhang, Q. H. Zhang, Z. H. Zhu, Y. Uwatoko, L. Gu, X. L. Dong, J. P. Sun, K. J. Jin, and J.-G. Cheng, Pressure-induced monotonic enhancement of  $T_c$  to over 30 K in superconducting  $\text{Pr}_{0.82}\text{Sr}_{0.18}\text{NiO}_2$  thin films, *Nat. Commun.* **13**, 4367 (2022).
- [22] K. Lee, B. Y. Wang, M. Osada, B. H. Goodge, T. C. Wang, Y. Lee, S. Harvey, W. J. Kim, Y. Yu, C. Murthy, S. Raghu, L. F. Kourkoutis, H. Y. Hwang, Pressure-induced monotonic enhancement of  $T_c$  to over 30K in superconducting  $\text{Pr}_{0.82}\text{Sr}_{0.18}\text{NiO}_2$  thin films, *Nature* **619**, 288 (2023).
- [23] H. Takagi, T. Ido, S. Ishibashi, M. Uota, S. Uchida, and Y. Tokura, Superconductor-to-nonsuperconductor transition in  $(\text{La}_{1-x}\text{Sr}_x)_2\text{CuO}_4$  as investigated by transport and magnetic measurements, *Phys. Rev. B* **40**, 2254 (1989).
- [24] Y. Kubo, Y. Shimakawa, T. Manako, and H. Igarashi, Transport and magnetic properties of  $\text{Tl}_2\text{Ba}_2\text{CuO}_{6+\delta}$  showing a  $\delta$ -dependent gradual transition from an 85-K superconductor to a nonsuperconducting metal, *Phys. Rev. B* **43**, 7875 (1991).
- [25] T. R. Chien, Z. Z. Wang, and N. P. Ong, Effect of Zn impurities on the normal-state Hall angle in single-crystal  $\text{YBa}_2\text{Cu}_{3-x}\text{Zn}_x\text{O}_{7-\delta}$ , *Phys. Rev. Lett.* **67**, 2088 (1991).
- [26] C. M. Duffy, S. J. Tu, Q. H. Chen, J. S. Zhang, A. Cuoghi, R. D. H. Hinlopen, T. Sarkar, R. L. Greene, K. Jin, N. E. Hussey, Evidence for spin-fluctuation-mediated superconductivity in electron-doped cuprates,

- arXiv:2502.13612.
- [27] M. Dion, S. Ghotb, G. Hardy, P. Fournier, Doping dependence of the nonlinear Hall resistivity in electron-doped  $\text{Pr}_{2-x}\text{Ce}_x\text{CuO}_{4\pm\delta}$ , arXiv:2410.16614.
  - [28] H. Kontani, K. Kanki, and K. Ueda, Hall effect and resistivity in high- $T_c$  superconductors: The conserving approximation, *Phys. Rev. B* **59**, 14723 (1999).
  - [29] H. Kontani, Anomalous transport phenomena in Fermi liquids with strong magnetic fluctuations, *Rep. Prog. Phys.* **71**, 026501 (2008).
  - [30] W. K. Huang, S. Hosoi, M. Culo, S. Kasahara, Y. Sato, K. Matsuura, Y. Mizukami, M. Berben, N. E. Hussey, H. Kontani, T. Shibauchi, Y. Matsuda, Non-Fermi liquid transport in the vicinity of nematic quantum critical point of  $\text{FeSe}_{1-x}\text{S}_x$  superconductor, *Phys. Rev. Research* **2**, 033367 (2020)
  - [31] L. Fanfarillo, E. Cappelluti, C. Castellani, and L. Benfatto, Unconventional Hall Effect in Pnictides from Interband Interactions, *Phys. Rev. Lett.* **109**, 096402 (2012).
  - [32] B. P. Stojković and D. Pines, Theory of the longitudinal and Hall conductivities of the cuprate superconductors, *Phys. Rev. B* **55**, 8576 (1997).
  - [33] F. Lechermann, J. Gondolf, S. Bötzel, and I. M. Eremin, Electronic correlations and superconducting instability in  $\text{La}_3\text{Ni}_2\text{O}_7$  under high pressure, *Phys. Rev. B* **108**, L201121 (2023).
  - [34] H. Liu, C. Xia, S. Zhou and H. Chen, Sensitive dependence of pairing symmetry on  $\text{Ni-}e_g$  crystal field splitting in the nickelate superconductor  $\text{La}_3\text{Ni}_2\text{O}_7$ , *Nat. Commun.* **16**, 1054 (2025).
  - [35] G. Heier, K. Park, and S. Y. Savrasov, Competing  $d_{xy}$  and  $s_{\pm}$  pairing symmetries in superconducting  $\text{La}_3\text{Ni}_2\text{O}_7$ : LDA+FLEX calculations, *Phys. Rev. B* **109**, 104508 (2024).
  - [36] Y.-B. Liu, J.-W. Mei, F. Ye, W.-Q. Chen, and F. Yang,  $s^{\pm}$ -Wave Pairing and the Destructive Role of Apical-Oxygen Deficiencies in  $\text{La}_3\text{Ni}_2\text{O}_7$  under Pressure, *Phys. Rev. Lett.* **131**, 236002 (2023).
  - [37] Y. Zhang, L.-F. Lin, A. Moreo, T. A. Maier, and E. Dagotto, Trends in electronic structures and  $s_{\pm}$ -wave pairing for the rare-earth series in bilayer nickelate superconductor  $R_3\text{Ni}_2\text{O}_7$ , *Phys. Rev. B* **108**, 165141 (2023).
  - [38] Q.-G. Yang, D. Wang, and Q.-H. Wang, Possible  $s_{\pm}$ -wave superconductivity in  $\text{La}_3\text{Ni}_2\text{O}_7$ , *Phys. Rev. B* **108**, L140505 (2023).
  - [39] K.-Y. Jiang, Y.-H. Cao, Q.-G. Yang, H.-Y. Lu, and Q.-H. Wang, Theory of Pressure Dependence of Superconductivity in Bilayer Nickelate  $\text{La}_3\text{Ni}_2\text{O}_7$ , *Phys. Rev. Lett.* **134**, 076001 (2025).
  - [40] Y. Gu, C. Le, Z. Yang, X. Wu, and J. Hu, Effective model and pairing tendency in bilayer Ni-based superconductor  $\text{La}_3\text{Ni}_2\text{O}_7$ , *Phys. Rev. B* **111**, 174506 (2025).
  - [41] Y. Zhang, L.-F. Lin, A. Moreo, T. A. Maier, and E. Dagotto, Structural phase transition,  $s_{\pm}$ -wave pairing, and magnetic stripe order in bilayered superconductor  $\text{La}_3\text{Ni}_2\text{O}_7$  under pressure, *Nat. Commun.* **15**, 2470 (2024).
  - [42] H. Sakakibara, N. Kitamine, M. Ochi, and K. Kuroki, Possible High  $T_c$  Superconductivity in  $\text{La}_3\text{Ni}_2\text{O}_7$  under High Pressure through Manifestation of a Nearly Half-Filled Bilayer Hubbard Model, *Phys. Rev. Lett.* **132**, 106002 (2024).
  - [43] J. Zhan, Y. Gu, X. Wu, and J. Hu, Cooperation between electron-phonon coupling and electronic interaction in bilayer nickelates  $\text{La}_3\text{Ni}_2\text{O}_7$ , *Phys. Rev. Lett.* **134**, 136002 (2025).
  - [44] J.-R. Xue and F. Wang, Magnetism and superconductivity in the  $t-J$  model of  $\text{La}_3\text{Ni}_2\text{O}_7$  under multiband Gutzwiller approximation, *Chin. Phys. Lett.* **41**, 057403 (2024).
  - [45] Y.-H. Tian, Y. Chen, J.-M. Wang, R.-Q. He, and Z.-Y. Lu, Correlation effects and concomitant two-orbital  $s_{\pm}$ -wave superconductivity in  $\text{La}_3\text{Ni}_2\text{O}_7$  under high pressure, *Chin. Phys. B* **109**, 165154 (2024).
  - [46] C. Lu, Z. Pan, F. Yang, and C. Wu, Interlayer-Coupling-Driven High-Temperature Superconductivity in  $\text{La}_3\text{Ni}_2\text{O}_7$  under Pressure, *Chin. Phys. Lett.* **132**, 146002 (2024).
  - [47] Z.-Y. Shao, Y.-B. Liu, M. Liu, F. Yang, Band structure and pairing nature of  $\text{La}_3\text{Ni}_2\text{O}_7$  thin film at ambient pressure, *Phys. Rev. B* **112**, 024506 (2025).
  - [48] C. Yue, J.-J. Miao, H. Huang, Y/ Hua, P. Li, Y. Li, G. Zhou, W. Lv, Q. Yang, F. Yang, H. Sun, Y.-J. Sun, J. Lin, Q.-K. Xue, Z. Chen, and Wei-Qiang, Correlated electronic structures and unconventional superconductivity in bilayer nickelate heterostructures, *Natl. Sci. Rev.* nwaf253 (2025).
  - [49] V. Christiansson, F. Petocchi, and P. Werner, Correlated Electronic Structure of  $\text{La}_3\text{Ni}_2\text{O}_7$  under Pressure, *Phys. Rev. Lett.* **131**, 206501 (2023).
  - [50] Z. Ouyang, J.-M. Wang, J.-X. Wang, R.-Q. He, L. Huang, and Z.-Y. Lu, Hund electronic correlation in  $\text{La}_3\text{Ni}_2\text{O}_7$  under high pressure, *Phys. Rev. B* **109**, 115114 (2024).
  - [51] S. Rye, N. Witt, and T. O. Wehling, Quenched pair breaking by interlayer correlations as a key to superconductivity in  $\text{La}_3\text{Ni}_2\text{O}_7$ , *Phys. Rev. Lett.* **133**, 096002 (2024).
  - [52] G. Duan, Z. Liao, L. Chen, Y. Wang, R. Yu, Q. Si, Orbital-selective correlation effects and superconducting pairing symmetry in a multiorbital  $t-J$  model for bilayer nickelates, arXiv:2502.09195.
  - [53] W. Qiu, Z. Luo, X. Hu, and D.-X. Yao, Pairing symmetry and superconductivity in  $\text{La}_3\text{Ni}_2\text{O}_7$  thin films, arXiv:2506.20727.
  - [54] D. Inoue, Y. Yamakawa, S. Onari, and H. Kontani, Unified mechanism of charge-density-wave and high- $T_c$  superconductivity protected from oxygen vacancies in bilayer nickelates, arXiv:2503.12925.
  - [55] Fukuyama H, Ebisawa H and Wada, Theory of Hall Effect. I: Nearly Free Electron, *Prog. Theor. Phys.* **42**, 494 (1969).
  - [56] R. Tazai, Y. Yamakawa, T. Morimoto, and H. Kontani, Quantum-metric-induced giant and reversible nonreciprocal transport phenomena in chiral loop-current phases of kagome metals, arXiv:2408.04233.
  - [57] C. Guo, C. Putzke, S. Konyzheva, X. Huang, M. Gutierrez-Amigo, I. Errea, D. C., M. G. Vergniory, C. Felser, M. H. Fischer, T. Neupert, P. J. W. Moll, Switchable chiral transport in charge-ordered kagome metal  $\text{CsV}_3\text{Sb}_5$ , *Nature* **611**, 461 (2022).
  - [58] Kontani and K. Yamada, Theory of Anomalous Hall Effect in Heavy Fermion System, *J. Phys. Soc. Jpn.* **63**, 2627 (1994).
  - [59] H. Kontani, R. Tazai, Y. Yamakawa, and S. Onari, Unconventional density waves and superconductivities in Fe-based superconductors and other strongly correlated electron systems, *Adv. Phys.* **70**, 355 (2021).
  - [60] O. K. Andersen, A. I. Liechtenstein, O. Jepsen, and F.

- Paulsen, LDA energy bands, low-energy hamiltonians,  $t'$ ,  $t''$ ,  $t_{\perp}(k)$ , and  $J_{\perp}$ , *J. Phys. Chem. Solids* **56**, 1573 (1995).
- [61] Z. Luo, X. Hu, M. Wang, Wéi Wú, and D.-X. Yao, Bi-layer Two-Orbital Model of  $\text{La}_3\text{Ni}_2\text{O}_7$  under Pressure, *Phys. Rev. Lett.* **131**, 126001 (2023).
- [62] S. Bötzel, F. Lechermann, J. Gondolf, and I. M. Eremin, Theory of magnetic excitations in the multilayer nickelate superconductor  $\text{La}_3\text{Ni}_2\text{O}_7$ , *Phys. Rev. B* **109**, L180502 (2024).
- [63] G. Grissonnanche, G. A. Pan, H. LaBollita, D. Ferenc Segedin, Q. Song, H. Paik, C. M. Brooks, E. Beauchesne-Blanchet, J. L. Santana Gonzalez, A. S. Botana, J. A. Mundy, B. J. Ramshaw, Electronic Band Structure of a Superconducting Nickelate Probed by the Seebeck Coefficient in the Disordered Limit, *Phys. Rev. X* **14**, 041021 (2024).